Computers and Chemical Engineering 153 (2021) 107412

Contents lists available at ScienceDirect

Computers and Chemical Engineering

journal homepage: www.elsevier.com/locate/compchemeng

# Mathematical modeling and analysis of microwave-assisted freeze-drying in biopharmaceutical applications

Jinwoo Park[a,b], Jae Hyun Cho[b], Richard D. Braatz[a,*]

[a] Department of Chemical Engineering, Massachusetts Institute of Technology, 77 Massachusetts Avenue, Cambridge, MA 02139, USA
[b] Department of Chemical and Biomolecular Engineering, Yonsei University, 50 Yonsei-ro, Seodaemun-gu, Seoul 03722, Republic of Korea

ARTICLE INFO

*Article history:*
Received 25 January 2021
Revised 13 June 2021
Accepted 14 June 2021
Available online 19 June 2021

*Keywords:*
Freeze drying
Microwave-assisted drying,
Microwave-assisted freeze drying
Bioprocessing
Primary drying
Biopharmaceutical manufacturing

ABSTRACT

Freeze drying is an essential unit operation for the storage of biopharmaceuticals, with its main weakness being the very long primary drying times required to sublimate all of the ice formed in the initial freezing step. This study investigates the use of microwave irradiation to reduce drying times. Mechanistic models are derived in a proposed freeze-drying process in which two energy transfer mechanisms – microwave irradiation and heat conduction – occur simultaneously. For this design, a mechanistic model derived in this article predicts an 83% reduction in primary drying time compared to conventional freeze drying. The influence of microwave power and design parameters associated with heat conduction parameters on the primary drying time are investigated and discussed. The model is implemented as open-source software in Julia and is available for engineers to use for designing such equipment.



## 1. Introduction

Mechanistic and data-driven modeling and the use of these models in optimization and control has gained increased attention in (bio)pharmaceutical manufacturing (Casola et al., 2019; Eberle et al., 2016; Kappatou et al., 2020; Liu and Papageorgiou, 2018; Papathanasiou et al., 2019). The use of computer-based methodologies is motivated by a desire to reduce process development time and drug manufacturing costs (Hong et al., 2018; Matsunami et al., 2018). Increased mechanistic modeling at various degrees of detail and using the model to analyze the impact of influential design parameters and their interactions are essential to achieve these objectives (Badr and Sugiyama, 2020).

Freeze-drying has become a key unit operation in biopharmaceutical manufacturing (Colucci et al., 2020; Fissore et al., 2019). This unit operation is extensively applied to biotherapeutics, including those developed in response to pandemics such as COVID-19 (e.g., see Kumar et al., 2020 for Remdesivir as COVID-19 treatment and Park et al., 2021 for mRNA vaccines). Freeze-drying preserves heat-sensitive products by avoiding exposure to a high temperature, which can potentially damage product quality (Muzzio and Dini, 2011). Freeze-drying is comprised of three steps: freezing, primary drying, and secondary drying. First, an aqueous solution with dissolved proteins and excipients is frozen with the objective of controlling the size distribution of the ice crystals (e.g., see Colucci et al., 2020 and references therein). Second, primary drying sublimates the ice under high vacuum conditions to leave pores behind that will accelerate secondary drying and enable rapid rehydration when the freeze-dried product is eventually used. After primary drying, the water content is about 3 to 5%. Finally, in secondary drying, much of the remaining water that is strongly bounded by absorption is removed to reduce the water content to 1 to 2%.

In conventional freeze-drying (CFD), the lengthy process time is the main drawback that has motivated the development of next-generation drying technologies (Langford et al., 2018). Primary drying takes most of the time in the freeze-drying steps, so the most effort has been in reducing the time of primary drying (Velardi and Barresi, 2008). Methods that have been proposed to reduce process time include moving from batch to continuous operation (Capozzi et al., 2019; Pisano et al., 2019) and applying microwave irradiation (Walters et al., 2014).

This article considers microwave-assisted freeze-drying (MFD) for primary drying, which is the most time-consuming step. This work is motivated by some experimental studies that showed significant reductions in overall drying times for various types of pharmaceutical materials by using microwave irradiation. The accelerated microwave-assisted drying of small-molecule pharmaceutical powders was demonstrated experimentally more than 15 years ago (Farrel et al., 2005; McMinn et al., 2007). More recent

* Corresponding author at: Department of Chemical Engineering, Massachusetts Institute of Technology, 77 Massachusetts Avenue, Cambridge, MA 02139, USA.
*E-mail address:* braatz@mit.edu (R.D. Braatz).

https://doi.org/10.1016/j.compchemeng.2021.107412
0098-1354/

**Nomenclature**

| | |
|---|---|
| $C$ | Mass concentration (kg/m$^3$) |
| $\hat{c}_p$ | Specific heat capacity (J/kgK) |
| $D$ | Knudsen diffusivity (m$^2$/s) |
| $E$ | Electric field strength (V/m) |
| $f$ | Frequency of microwave (Hz) |
| $H_b$ | Heat generation from the bottom shelf (W/m$^2$) |
| $H_{ice}$ | Volumetric heat generation to the ice by microwave (W/m$^3$) |
| $H_w$ | Volumetric heat generation to the water by microwave (W/m$^3$) |
| $H_v$ | Volumetric heat generation by microwave (W/m$^3$) |
| $\Delta H$ | Specific enthalpy (J/kg) |
| $h$ | Heat transfer coefficient (W/m$^2$K) |
| $k$ | Thermal conductivity (W/mK) |
| $k_m$ | Internal mass transfer coefficient (1/s) |
| $L$ | Depth of bottom (m) |
| $M$ | Molecular weight of water (kg/kmol) |
| $N$ | Mass flux (kg/m$^2$s) |
| $P$ | Vapor pressure (Pa) |
| $p$ | Portion of the component |
| $q$ | Heat flux (W/m$^2$) |
| $R$ | Universal gas constant (J/kmolK) |
| $r$ | Increase rate of shelf temperature (K/s) |
| $T$ | Temperature (K) |
| $t$ | Time (s) |
| $X(t)$ | Position of moving boundary (m) |
| $x$ | Axial coordinate (m) |
| $\varepsilon$ | Void fraction of dried layer |
| $\varepsilon_0$ | Permittivity of free space (F/m) |
| $\varepsilon\prime$ | Relative loss factor |
| $\rho$ | Density (kg/m$^3$) |

*Superscript*

| | |
|---|---|
| 0 | Initial condition |
| int | Interface |
| equil. | Equilibrium |

*Subscripts*

| | |
|---|---|
| 1 | Region 1 |
| 2 | Region 2 |
| bottom | Bottom |
| bw | Bound water |
| e | Effective |
| shelf | Shelf |
| sub | Sublimation |
| w | Water vapor |
| vap | Vapor |

experiments in microwave-assisted drying have been applied to biological materials, including bacteria and enzymes, which were shown to survive being exposed to microwave irradiation during the drying (Ambros et al., 2016; de Jesus and Filho, 2011). Very recently, MFD has been successfully applied to generate freeze-drying material for monoclonal antibodies (Gitter et al., 2019), which are one of the major classes of biologic drugs. A significant reduction of 75% in drying time was observed, while still producing a product with high quality and long-term stability (Gitter et al., 2018).

The mathematical modeling of MFD for biopharmaceutical products is not yet well developed. The development of process models for biopharmaceutical applications typically has three goals: (1) accuracy, (2) simplicity, and (3) interpretability (Severson et al., 2015). Industry applies simple empirical correlations related to parameters such as moisture content and drying time, which can be accurate and simple, but are not readily interpretable. The main objective of this article is to derive a mathematical model for MFD for biopharmaceutical products that meets all three goals, by incorporating mechanistic information on the interaction of microwave irradiation on the material during drying, as well as on heat and mass transfer.

The mechanistic modeling of CFD of foods is reasonably well developed (Fan et al., 2019; Kawasaki et al., 2019). Litchfield and Liapis (1979) proposed the first mechanistic model for freeze-drying, which became widely used in the literature without any major modifications (Liapis and Bruttini, 1995; Mascarenhas et al., 1997; Millman et al., 1985; Pikal et al., 2005). The model has been validated in pilot-scale experiments (Hottot et al., 2006), and simplified versions of the model have been published (Velardi and Barresi, 2008). Also, the freeze-drying model has been modified to replace conventional heating by microwave irradiation for accelerating drying times (Witkiewicz and Nastaj, 2010).

This study derives a mechanistic model for primary drying that includes both microwave irradiation and conventional heat conduction (MFD and CFD), with the MFD part of the model validated with experimental data in the literature for a monoclonal antibody product. The purpose of the model is to gain insight into the relationship between the operating conditions and the drying time. The model is designed to be computationally inexpensive enough to be implementable in real-time nonlinear model predictive control algorithms (Nagy and Braatz, 2011) and for early-stage process design. The focus is on primary drying as this step is the main contribution to the overall drying time. The mechanistic model is solved using the finite volume method in Julia, which is an open-source software platform optimized for numerical calculations.[1] The results of microwave irradiation and its combination with conventional heating are compared to CFD, and parametric sensitivity analysis is carried out to reveal its features.

## 2. Model description

The mechanistic model is described in this section. Fig. 1 describes the model framework for the study (Litchfield and Liapis, 1979; Velardi and Barresi, 2008; Witkiewicz and Nastaj, 2010). As discussed in the Introduction, a mechanistic model is already widely used for the primary drying step of freeze-drying (Litchfield and Liapis, 1979). However, this complex model has a high computational cost and a large number of model parameters that are not directly measurable, so a simplified model has been proposed that presents a good approximation (Velardi and Barresi, 2008). This article builds on the simplified model by introducing additional equations for describing the effects of microwave irradiation. The finite volume method is used for the calculation, by using VoronoiFVM.jl in Julia. Finally, three different types of freeze-drying configurations are compared: CFD with heating from the bottom shelf, MFD using microwave irradiation for heating, and hybrid freeze-drying (HFD), which uses both methods.

The full and simplified models can be expressed in a mathematical form with the system boundary and its components illustrated in Fig. 2 (Litchfield and Liapis, 1979; Witkiewicz and Nastaj, 2010). The core of the primary drying model is based on the past research that models two different regions: dried and frozen (Litchfield and Liapis, 1979). The dried region contains water vapor with pressure under the high vacuum created by a vacuum pump. The frozen region comprises ice and solute. At the solid-gas interface, the sublimation of ice and vaporization of bound water occurs. The energy for the drying is supplied from the bottom shelf

[1] The software is released with an open-source license. https://github.com/jinkel7/microwave-freeze-drying

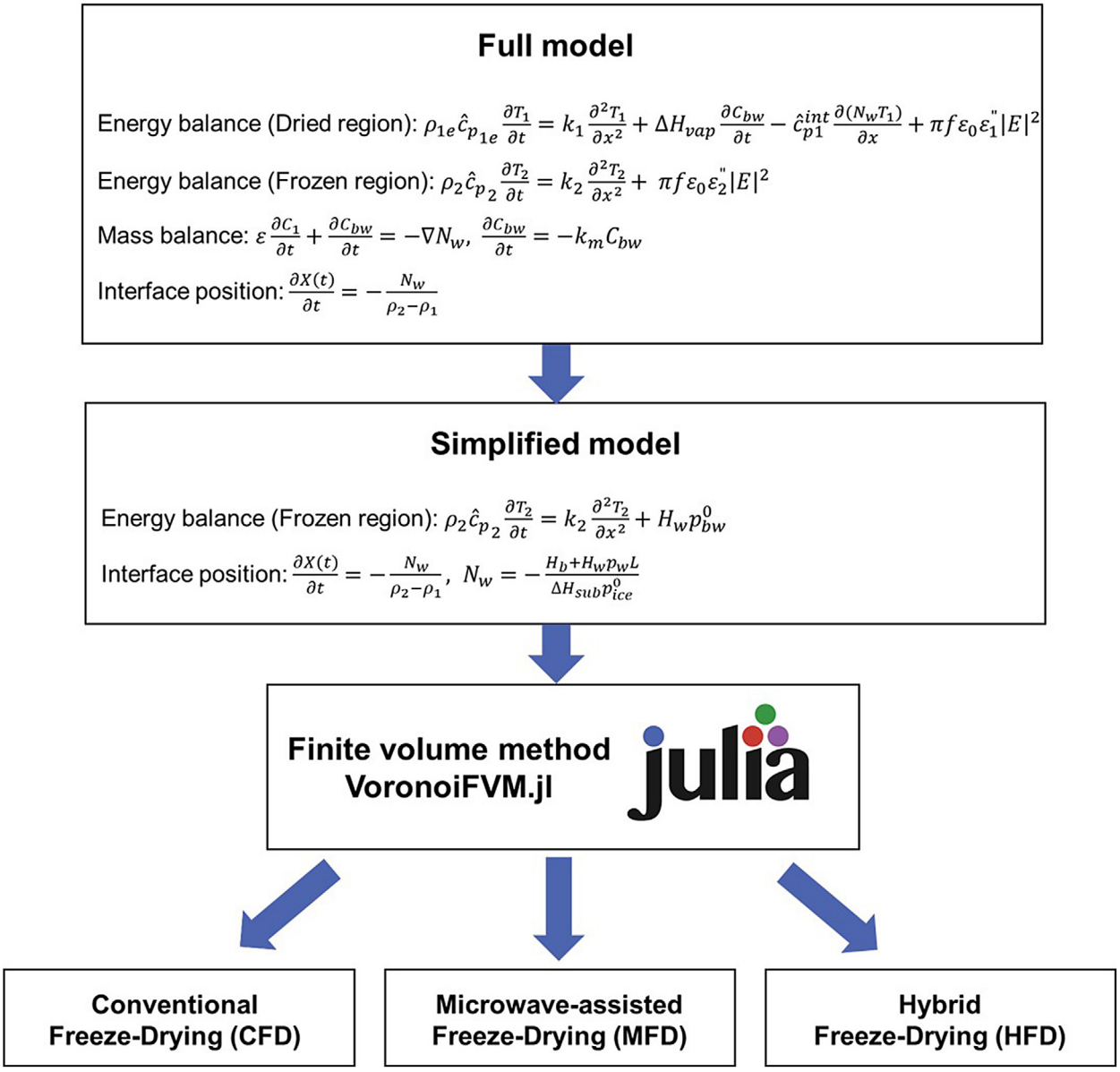


**Fig. 1.** Model framework (Litchfield and Liapis, 1979; Velardi and Barresi, 2008; Witkiewicz and Nastaj, 2010).

by conduction and/or into the bulk material by microwave irradiation. The freeze-drying model of Witkiewicz and Nastaj (2010) considers microwave irradiation, but neglects bound water and simplifies the mass transfer of the dried region.

The literature cited in this article makes and justifies a set of assumptions on the model geometry concerning wall effects, container boundary effects, etc. that are very well established to hold in both modeling and experiments across many decades of lyophilization literature by different research groups for different lyophilizers (e.g., Litchfield and Liapis, 1979; Velardi and Barresi, 2008; Witkiewicz and Nastaj, 2010). The low magnitude of radial gradients is well established in the literature (e.g., Velardi and Barresi, 2008). The heat source for thermal conduction is right below the bottom of the vial, where the temperature is uniform in the radial direction. The condition at the top of the vial of a vacuum is uniform in the radial direction. The microwave irradiation is spatially uniform in the radial direction as well. Wall/container boundary effects are small, since the thermal conductivity of glass in the vial walls is low, so there is no preferential thermal conduction up the glass walls, and the vials are surrounding by a vacuum which is nearly a perfect insulator. When the dominant sources and sinks have no radial directionality, large radial gradients do not form.

This one-dimensional system has a moving boundary where the interface continuously moves in accordance with the sublimation rate. In the simplified model (Velardi and Barresi, 2008), the influence of the dried region is neglected, since the gas is under a high vacuum and the overall solid mass is low due to the high porosity (e.g., $<$ 80%, Sheehan and Liapis, 1998). In addition, the vaporization of bound water is neglected because the ice sublimation is much high (e.g., $>$ 95% of the total mass of $H_2O$ that enters the vapor phase, Velardi and Barresi, 2008) during primary drying, and the heats of sublimation and vaporization are comparable in magnitude (within 10%). Also, the inert gas in the dried region is ignored due to high vacuum conditions, and the thermal radiation from the top and the sidewall of the vial is neglected, since the amount is relatively negligible (Velardi and Barresi, 2008). Both the

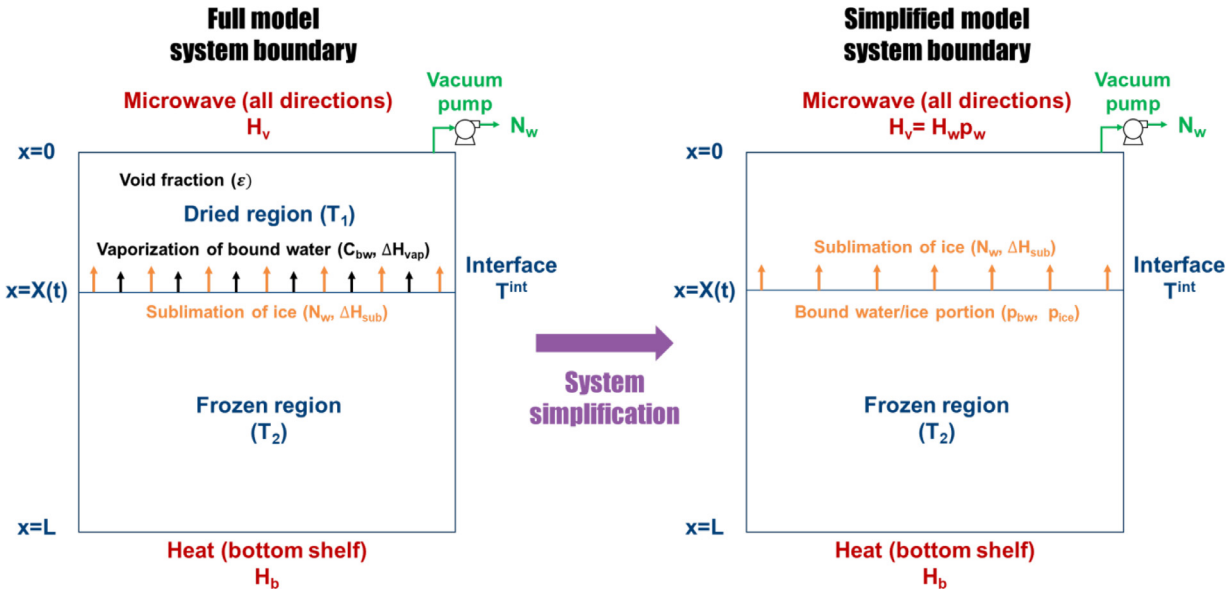


**Fig. 2.** System boundary of the full and simplified models for microwave irradiation. The full model schematic on the left is by Litchfield and Liapis (1979) with microwave irradiation term of Witkiewicz and Nastaj (2010), and the simplified model schematic on the right is proposed in this article.

full and simplified models (Litchfield and Liapis, 1979; Velardi and Barresi, 2008) make the additional assumptions that

- The interface thickness is infinitesimal.
- No vapor transfer occurs from the bottom and the sidewall.
- At the solid-gas interface, the concentration of water vapor is in equilibrium with the ice.
- In the dried region, the movement of moisture is sufficiently slow that the solid matrix and the gas are in thermal equilibrium.
- The frozen region has uniform properties for mass and heat transfer, and the proportion of dissolved gases are neglected.
- The heat transfer limitation through the glass bottom of the vial is neglected, i.e., the heat is directly transferred from the bottom shelf, since the effect is small compared to other heat transfer limitations.

For the effect of microwave irradiation, the generated electrical field is spatially uniform, and its polarization is perpendicular to the surface (Witkiewicz and Nastaj, 2010). The aforementioned assumptions justify that the PDEs of the full and simplified models to be built in this article is enough to describe by one axial spatial coordinate.

The next section summarizes the full mechanistic model of Litchfield and Liapis (1979) to serve as a basis for comparison to the simplified mechanistic model proposed in the subsequent section, especially with regard to how additional assumptions modify the governing equations.

### 2.1. Full model

#### 2.1.1. Mass balance

The mass balance of the system is expressed as

$$\varepsilon \frac{\partial C_1}{\partial t} + \frac{\partial C_{bw}}{\partial t} = -\nabla N_w \tag{1}$$

where $\varepsilon$ denotes the void fraction of the dried layer, $C_1$ denotes the mass concentration of the dried region, $C_{bw}$ denotes the mass concentration of bound water, and $N_w$ denotes the mass flux of water vapor. Equation (1) indicates the balance between ice sublimation, bound water vaporization, and vacuum pump discharging.

The mass concentration of the dried region $C_1$ is assumed to follow the ideal gas law:

$$C_1 = \frac{M}{RT_1} P_w \tag{2}$$

where $M$ denotes the molecular weight of water, $R$ denotes universal gas constants, $T_1$ denotes the temperature of the dried region, and $P_w$ denotes the vapor pressure of water.

For the bound water,

$$\frac{\partial C_{bw}}{\partial t} = -k_m \left( C_{bw} - C_{bw}^{equil.} \right) \approx -k_m C_{bw} \tag{3}$$

where $k_m$ denotes the internal mass transfer coefficient and $C_{bw}^{equil.}$ denotes the mass concentration of bound water. At the solid-gas interface, bound water is in equilibrium with the water vapor at high vacuum, and the term involving $C_{bw}^{equil.}$ can be dropped, which has been experimentally verified (Sadikoglu and Liapis, 1997; Sheehan and Liapis, 1998).

The molar flux of water vapor (Pikal et al., 2005) is

$$N_w = -\frac{M}{RT_1} D_w \nabla P_w \tag{( 4)}$$

where $D_w$ is the Knudsen diffusivity of the water vapor. This expression of diffusivity applies due to the high vacuum conditions (Hottot et al., 2006).

The initial and boundary conditions for the mass balance are

$$P_w = P_w^0 \text{ at } t = 0 \tag{5}$$

$$C_{bw} = C_{bw}^0 \text{ at } t = 0 \tag{6}$$

$$P_w = P_w^0 \text{ at } t > 0, x = 0 \tag{7}$$

$$P_w = P_w\left(T^{int}\right) \text{ at } t > 0, \ x = X(t) \tag{8}$$

where superscript 0 denotes initial condition, $T^{int}$ denotes the interface temperature, and $X(t)$ denotes the position of the moving boundary.

*2.1.2. Energy balance*

The energy balance is more complicated than the mass balance because the two different regions have different forms of the equation. The basis of the energy balance equation is expressed as

$$\rho \hat{c}_p \frac{\partial T}{\partial t} = -\nabla q + H_v \tag{9}$$

where $\rho$ denotes the density, $\hat{c}_p$ denotes the specific heat capacity, $q$ denotes the heat flux, and $H_v$ denotes the volumetric heat generation by microwave. The density and the specific heat capacity are assumed as constant. In addition, viscous dissipation and pressure variation are ignored.

The system uses a microwave that $H_v$ is expressed as

$$H_v = \pi f \varepsilon_0 \varepsilon'' |E|^2 \tag{10}$$

where $f$ denotes the frequency of microwave, $\varepsilon_0$ denotes the permittivity of free space, $\varepsilon''$ denotes relative loss factor, and $E$ denotes the electric field strength.

According to equation (9), the energy balance of the dried region is expressed as

$$\rho_{1e} \hat{c}_{p_{1e}} \frac{\partial T_1}{\partial t} = k_1 \frac{\partial^2 T_1}{\partial x^2} + \Delta H_{vap} \frac{\partial C_{bw}}{\partial t} - \hat{c}_{p1}^{int} \frac{\partial (N_w T_1)}{\partial x} + \pi f \varepsilon_0 \varepsilon''_1 |E|^2 \tag{11}$$

where$\rho_{1e}$ denotes the effective density of the dried region, $\hat{c}_{p_{1e}}$ denotes the effective specific heat capacity of the dried region, $k_1$ denotes the thermal conductivity of the dried region, $\Delta H_{vap}$ denotes the specific enthalpy of vaporization, and $\hat{c}_{p1}^{int}$ denotes the specific heat capacity of the dried region near the interface. Equation (11) implies time and axial temperature variance with bound water vaporization, ice sublimation, and microwave.

The energy balance for the frozen region is

$$\rho_2 \hat{c}_{p_2} \frac{\partial T_2}{\partial t} = k_2 \frac{\partial^2 T_2}{\partial x^2} + \pi f \varepsilon_0 \varepsilon''_2 |E|^2 \tag{12}$$

where $\rho_2$ denotes the density of the frozen region,$\hat{c}_{p_2}$ denotes the specific heat capacity of the frozen region, and $k_2$ denotes the thermal conductivity of the frozen region. The last term in equation (12) is the volumetric energy input from the microwave, whereas the heat flux from the bottom shelf is considered in the boundary conditions.

The initial and boundary conditions for the energy balances for the dried and frozen regions are

$$T_1 = T_1^0 \text{ at } t = 0,\ 0 < x < X(t) \tag{13}$$

$$-k_1 \frac{\partial T_1}{\partial x} = 0 \text{ at } t > 0,\ x = 0 \tag{14}$$

$$T_1 = T^{int} \text{ at } t > 0,\ x = X(t) \tag{15}$$

$$T_2 = T_2^0 \text{ at } t = 0,\ X(t) < x < L \tag{16}$$

$$T_2 = T^{int} \text{ at } t > 0,\ x = X(t) \tag{17}$$

$$-k_2 \frac{\partial T_2}{\partial x} = H_b \text{ at } t > 0,\ x = L \tag{18}$$

where $L$ denotes the depth of bottom, and $H_b$ denotes the heat generation from the bottom shelf.

The heat flux from the bottom is expressed as

$$H_b = h\left(T_{shelf} - T_{bottom}\right) \tag{19}$$

where $h$ denotes the heat transfer coefficient, $T_{shelf}$ denotes the temperature of the shelf, and $T_{bottom} = T_2(x = L)$ denotes the temperature at the bottom of the vial. The determination of the heat transfer coefficient from experimental data is well explained in the literature (Pikal et al., 2005).

The velocity of the moving interface can be calculated from the rate of sublimation:

$$\frac{\partial X(t)}{\partial t} = -\frac{N_w|_{x=X(t)}}{\rho_2 - \rho_1} \tag{20}$$

where $N_w|_{x=X(t)}$ is the mass flux of water vapor at the interface, which is equivalent to the sublimation rate.

The sublimation rate at the interface is determined as

$$N_w|_{x=X(t)} = \frac{k_2 \nabla T_2 - k_1 \nabla T_1}{\left(\hat{c}_{p1}^{int} - \frac{\rho_2 \hat{c}_{p_2} - \rho_1 \hat{c}_{p_1}}{\rho_2 - \rho_1}\right) T^{int} + \Delta H_{sub}} \tag{21}$$

where equation (21) is based on the energy balance, which is explained in published work (Velardi and Barresi, 2008).

The full mechanistic model derived here is most closely related to two past models. We modify the model of Litchfield and Liapis (1979), which considers only CFD, to include the microwave irradiation term from the model of Witkiewicz and Nastaj (2010). To understand the system precisely, the full mechanistic model presented here is based on Litchfield and Liapis (1979) rather than the model of Witkiewicz and Nastaj (2010), which neglects some factors, in particular, their equation corresponding to our equation (11) ignores the bound water term, and their mass balance of the dried region was simplified by neglecting porosity and bound water, so their equations corresponding to our equations (1) to (8) are very different.

*2.2. Simplified model*

The detailed transient model above has a complex structure and requires many parameters to be determined for a process with limited measurements. This section derives a simplified model for primary drying that modifies a model by Velardi and Barresi (2008) to include microwave irradiation. The key ideas in the simplified model are assuming quasi-stationary conditions for the two regions because of the slow dynamics of the process, and using only the heat flux for the sublimation of the ice (Giordano et al., 2011). Fig. 3 is a schematic of the calculation procedure for the model extended to include microwave irradiation. First, the energy supplied from the bottom shelf and microwave irradiation is used to increase the temperature of the ice. After achieving sublimation temperature at the bottom, the heat provided is only used for the sublimation.

For the energy balance of the frozen region, during rising temperature, equation (12) is used with an abbreviated form of the microwave irradiation:

$$\rho_2 \hat{c}_{p_2} \frac{\partial T_2}{\partial t} = k_2 \frac{\partial^2 T_2}{\partial x^2} + H_v \tag{22}$$

where the initial and boundary conditions are defined according to equations (13)–(18) by

$$-k_2 \frac{\partial T_2}{\partial x} = 0 \text{ at } t > 0,\ x = 0 \tag{23}$$

$$-k_2 \frac{\partial T_2}{\partial x} = H_b \text{ at } t > 0,\ x = L \tag{24}$$

$$T_2 = T_2^0 \text{ at } t = 0,\ 0 < x < L \tag{25}$$

The values for $H_b$ can be calculated using equation (19) with a shelf temperature treated in this study of

$$T_{shelf}(t) = rt + T_{shelf}^0 \tag{26}$$

where $r$ is the rate of rise in the shelf temperature.

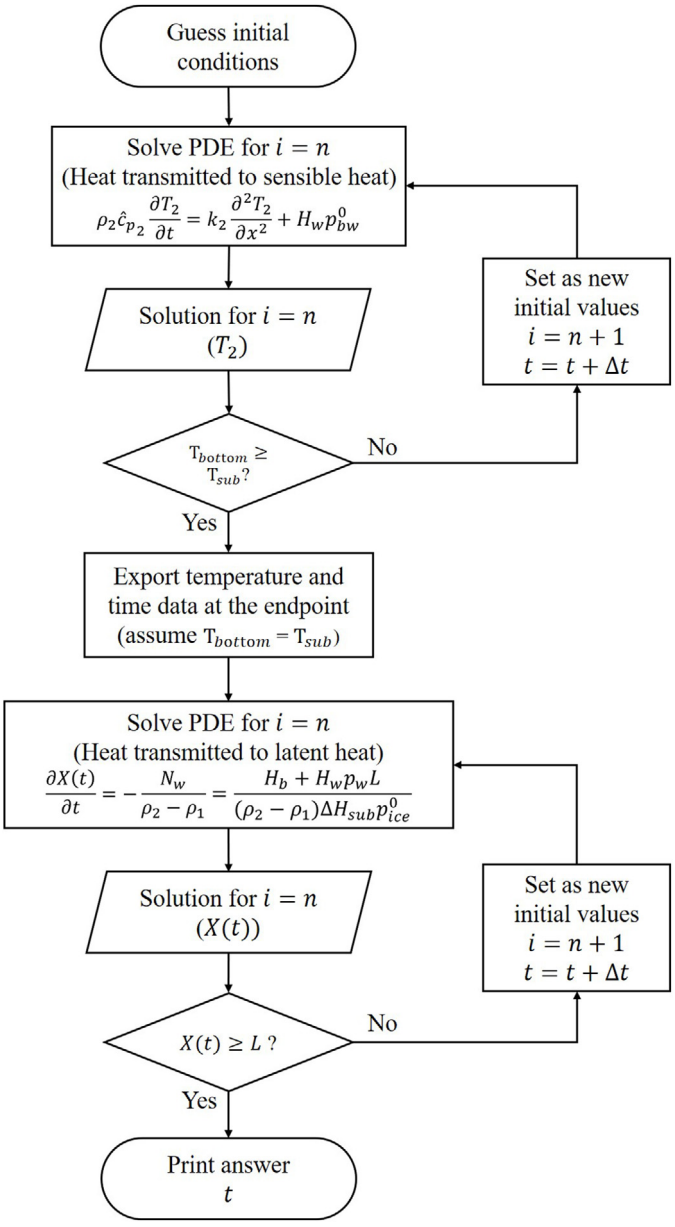


**Fig. 3.** Calculation procedure for the simplified model.

Unlike the original simplified model of Velardi and Barresi (2008), which ignored the bound water during primary drying, the microwave irradiation affects water and ice differently, which is modeled here by

$$H_v = H_{ice} p_{ice}^0 + H_w p_{bw}^0 \approx H_w p_{bw}^0 \text{ for } t \leq t_{sub} \tag{27}$$

where $p$ denotes the portion of the component and $t_{sub}$ denotes the time sublimation initializes. The microwave term can be confined to the water because the microwave irradiation has a vastly higher effect on the water than ice (Matzler, 1987),

$$\varepsilon\prime_{ice} \approx \varepsilon\prime_{water}/190,000 \tag{28}$$

In the sublimation stage, the microwave irradiation term is comprised as

$$H_v = H_{ice} p_{ice} + H_w p_w \approx H_w p_w \text{ for } t \quad t > t_{sub} \tag{29}$$

where $p_w$ is the parameter for the water-related portion in microwave heating during sublimation. This parameter describes the complex system, including water vapor and bound water.

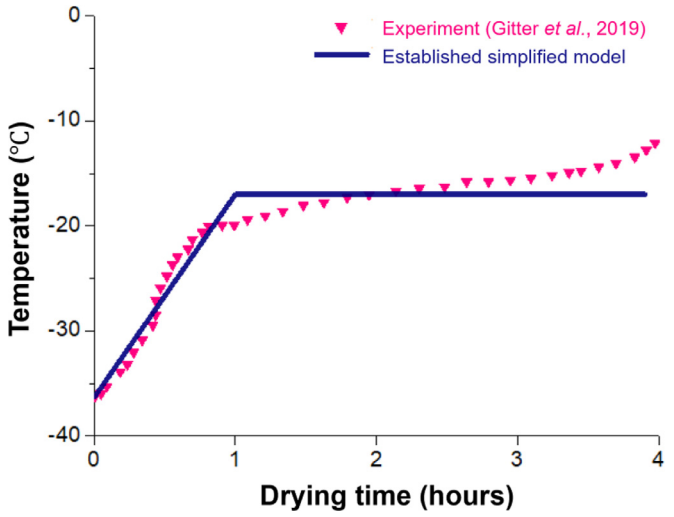


**Fig. 4.** Comparison of experimental data for the temperature at the bottom of the vial with a simplified model. For the simplified model, the bottom temperature is increasing to the sublimation temperature during the initial ramp, and the ice is sublimating with the bottom temperature equal to the sublimation temperature in the plateau region.

Then, equation (20) is reorganized to calculate the moving boundary,

$$\frac{\partial X(t)}{\partial t} = -\frac{N_w}{\rho_2 - \rho_1} = \frac{H_b + H_w p_w L}{(\rho_2 - \rho_1)\Delta H_{sub} p_{ice}^0} \text{ for } t > t_{sub} \tag{30}$$

where sublimation occurs due to heat transmission through the bottom shelf, and volumetric microwave heat generation.

The simplified model can be approximated by some analytical expressions. For $H_b + H_w p_w L$ that is nearly constant (e.g., if $H_w p_w L > H_b$), $X(t)$ will grow linearly. Under the experimental conditions of $H_w p_w L \gg H_b$ (for example, when $H_b = 0$ as in Gitter et al. (2019)), an approximate analytical solution to equation (30) during primary drying is

$$X(t) = 0 \text{for} t \leq t_{sub} \tag{31}$$

$$X(t) = \frac{\left(H_{b,ave} + H_w p_w L\right)t}{(\rho_2 - \rho_1)\Delta H_{sub} p_{ice}^0} \text{ for } t > t_{sub} \tag{32}$$

where $H_{b,ave}$ is the average value of $H_b$ during the experiment. An analytical solution for the temperature can be derived as

$$T_2 = -\frac{r\rho_2 \hat{c}_{p_2} + H_w p_{bw}^0}{2k_2}(x^2 - L^2) + \frac{2aLk_2}{h} + rt + T_{shelf}^0 \text{ for } t \leq t_{sub} \tag{33}$$

$$T_2 = T_{sub} \text{ for } t > t_{sub} \tag{34}$$

where the details of derivation are shown in an Appendix. This approximately linear relationship during primary drying can be seen in Fig. 4.

Fig. 4 compares the simplified model with MFD experimental data from a past study (Gitter et al., 2019). Table 1 lists the parameters used in the simplified model, with citations given for the model parameters from the literature and with the $H_w$, $p_w$, and $L$ fit to the experimental data. The simplified model captures the temperature ramp, the transition to the plateau region, and the overall drying time quite accurately, with the main differences being that the experimental temperature profile has a smoother transition from the temperature ramp to the plateau and an upwards drift during the time that the simplified model predicts a plateau.

**Table 1**
Parameters for the validation

| Parameter | Value |
|---|---|
| $\rho_1$ (Velardi and Barresi, 2008) | 63 kg/m$^3$ |
| $\rho_2$ (Velardi and Barresi, 2008) | 917 kg/m$^3$ |
| $\hat{c}_{p_2}$ (Velardi and Barresi, 2008) | 1,967.8 J/kgK |
| $\Delta H_{sub}$ (Velardi and Barresi, 2008) | 2.840 $\times$ 10$^6$ J/kg |
| $H_w$ | 242,345 W/m$^3$ |
| $h$ (Hottot et al., 2006) | 65 W/m$^2$K |
| $k_2$ (Velardi and Barresi, 2008) | 2.30 W/mK |
| $p^0_{bw}$ | 0.04 |
| $p_w$ | 0.92 |
| $L$ | 0.042 m |
| $T^0_2$ (Gitter et al., 2019) | 236.85 K |
| $T_{sub}$ (Gitter et al., 2019) | 256.15 K |

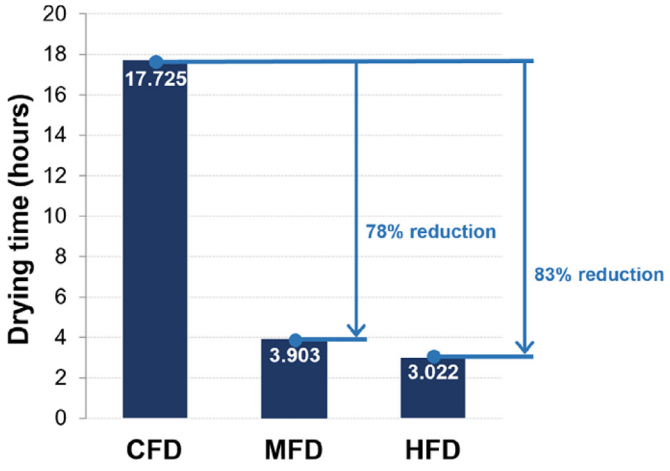


**Fig. 5.** Calculated drying time of each freeze-drying type.

Of the various features, the most important for this particular design study is that the overall drying time of ~ 4 hours predicted by the model is within the accuracy of the experimental data.

## 3. Comparison between different freeze-drying types

This section applies the simplified model to compare the primary drying performance for three different freeze-drying types: CFD, MFD, and HFD. The shelf temperature is set as a general experimental condition, 236.85 K initially and rising at 1 K/min, finally reaching 281.85 K. Fig. 5 displays the calculated drying time of each freeze-drying type. MFD has a drying time of ~3.9 hours, which is 78% lower than CFD. These model predictions are highly consistent with the experimentally reported reduction in the drying time of "over 75%" reported by Gitter et al. (2018) in biopharmaceutical freeze-drying experiments. Furthermore, our model predicts that HFD would have an 83% lower drying time than CFD, which is ~23% faster drying time than MFD. These model predictions strongly motivate the design and development of freeze-drying equipment that is able to use both microwave irradiation and conventional conductive heating from the bottom shelf.

Fig. 6 plots the spatiotemporal temperature variation during the temperature ramp in Fig. 4 for the three types of freeze drying, which is before the bottom temperature reaches the sublimation temperature (cf. Fig. 3). CFD has a more rapid temperature rise at the bottom than the other freeze-drying types where all or most of the energy comes from microwave heating in the bulk. MFD has a constant increase in temperature with time with no spatial variation, because the microwave irradiation heats the overall region consistently and uniformly. HFD is intermediate in the spatial variation of temperature while reaching the sublimation temperature more quickly (0.55 h) due to having both conventional and microwave heating. Due to having a spatial gradient, CFD reaches the sublimation temperature 26% faster (0.74 h) than MFD (1.00 h), which is a limitation of the simplified model for describing CFD that the initial sublimation time highly depends on the bottom temperature. Even if sublimation started earlier in CFD, MFD has a much faster primary drying time due to much higher energy supplied from microwave irradiation during the sublimation (cf. Fig. 5 and Table 2).

**Table 2**
Comparison of energy transmission rates.

| Energy source | Value |
|---|---|
| Microwave ($H_wL$) | 10,178 W/m$^2$ |
| in raising the temperature ($H_w p^0_{bw} L$) | 407 W/m$^2$ |
| in sublimation ($H_w p_w L$) | 9,567 W/m$^2$ |
| Bottom shelf ($H_b$) | Up to 1,671 W/m$^2$ |

Table 2 describes calculated energy transmission from microwave irradiation and bottom shelf heating, which both in terms of flux with respect to the cross-sectional area so as to be placed on the same basis. The microwave irradiation uniformly provided 242,345 W/m$^3$ of energy, which is equivalent to 10,178 W/m$^2$ for this 0.042 m depth of material in the vial. Recall that almost no energy from microwave irradiation is transferred to the ice, and instead is transferred to the bound water, which is essential for heating. During the sublimation, sublimated water vapor heavily affects the energy transmission of the microwave irradiation (cf. the second and third rows of Table 2). On the other hand, the bottom shelf transmits energy up to 1,671 W/m$^2$. The energy provided from the bottom shelf varies according to the temperature changes in the frozen region and the bottom shelf. According to the results, microwave energy transfer is not as effective as direct heat conduction during the time period that the temperature is rising. However, microwave irradiation has a much stronger effect on sublimation, which is up to 5.72 times larger than direct conductive heat transfer.

## 4. Parametric sensitivity analysis for HFD

HFD uses both heating mechanisms of CFD and MFD to enhance the speed of primary drying. Investigating controllable parameters is helpful for the further development of biopharmaceutical freeze-drying. Thus, parametric sensitivity analysis is conducted for HFD according to the developed mechanistic model for three potentially important design parameters: microwave power and the temperature difference at and depth of the bottom of the vial. Each parameter is varied by $\pm$10 to 30% compared to the base case.

The primary drying time is approximately inversely proportional to the microwave power (see Fig. 7). For instance, for a 30% increase in microwave power from the base case, the primary drying time is reduced by about 18% from the base case, which is a bit less than a perfect inverse proportionality (which would be $1 - 1/1.3 = 23\%$). For a 30% reduction in microwave power from the base case, the primary drying time increases by ~30% from the base case, which is slightly less than a perfect inverse proportionality ($1/0.7 - 1 = 43\%$). The inverse proportionality is not perfect but is a rough rule of thumb for back-of-the-envelope estimates, but the deviation from this short-cut estimate will vary with the base microwave power and how large of a deviation is considered.

Fig. 8 shows that the primary drying time is approximately a linear function of the temperature difference at the bottom of the vial, which is proportional to the energy flux from the bottom of the vial. The base case has a 45 K difference in temperature between the ice and the bottom shelf when the sublimation occurs. For a 30% increase in the temperature difference, the primary dry-

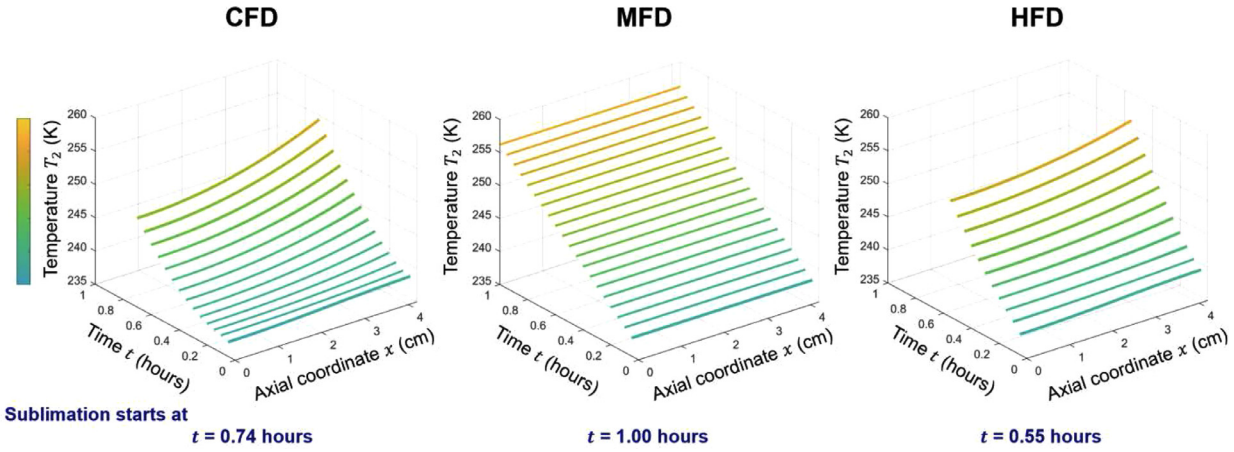


**Fig. 6.** Spatiotemporal variation in the temperature until the sublimation begins for conventional freeze drying (CFD), microwave-assisted freeze drying (MFD), and hybrid freeze drying (HFD). The time between adjacent spatial temperature profiles is 0.05 hr. The units of time and axial coordinate are reported in hours and centimeters here for better readability.

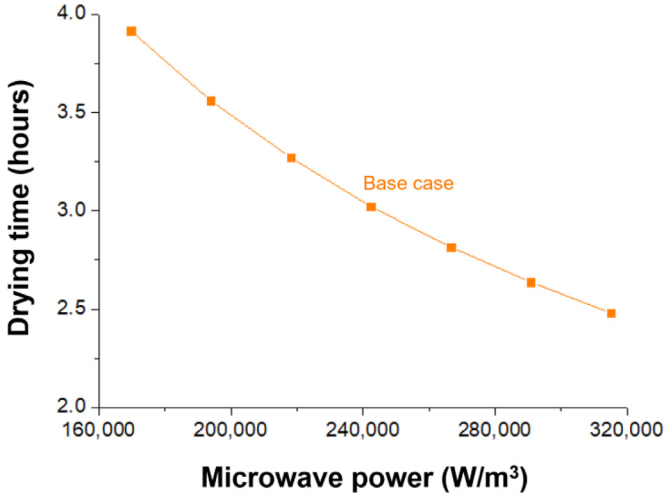


**Fig. 7.** Drying time vs. microwave power.

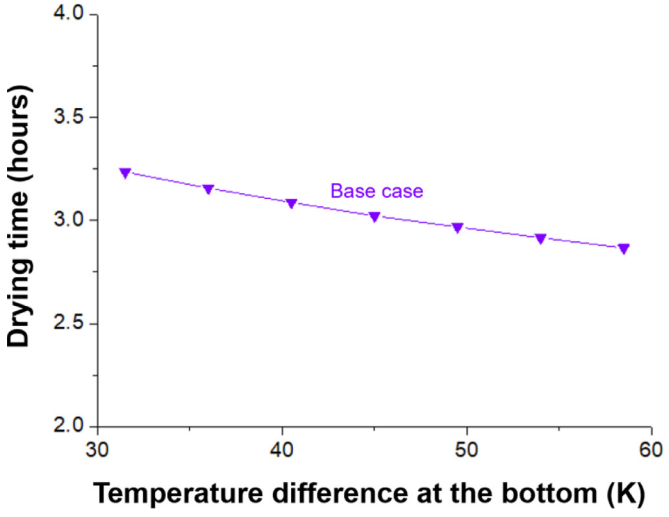


**Fig. 8.** Drying time vs. temperature difference at the bottom.

ing time is reduced by 5.1%, whereas a 30% decrease in the temperature difference results in a 7.1% reduction in the primary drying time. The primary drying time is weakly sensitive to the temperature difference at the bottom of the vial during HFD since microwave power provides most of the energy for drying.

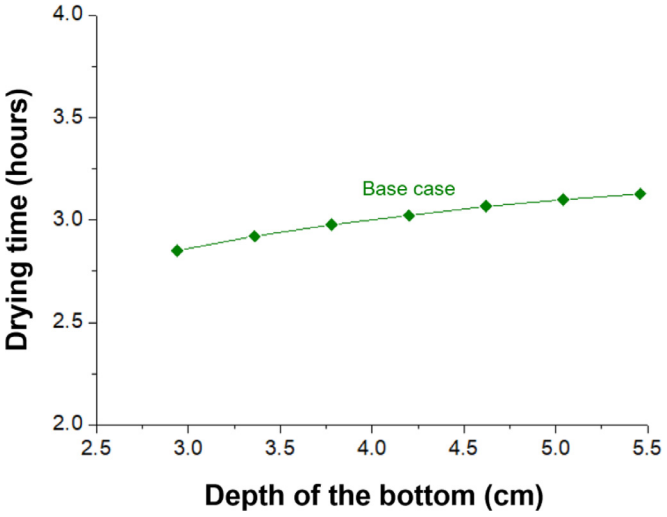


**Fig. 9.** Drying time vs. depth of the bottom.

The primary drying time also has a relatively weak dependency on the depth of the bottom of the vial (Fig. 9). Increasing the depth of the bottom by 30% from the base case only increases the primary drying time by 3.5%, and a 30% decrease results in a 5.7% reduction in primary drying time. In contrast to the CFD, which is known to be highly impacted by the depth of the bottom of the vial, its effect on the primary drying time for HFD is quite small. Again, this weak dependence is because most of the energy for drying comes from the microwave irradiation.

Overall, the parametric sensitivity analysis confirms our expectation that the microwave power is the primary design variable to consider when designing freeze-drying equipment that uses both microwave irradiation and conventional heat conduction. Because the energy transfer from microwave irradiation is primarily to bound and vaporized water, that energy transfer is transmitted throughout the volume of the ice, which is much more effective than heat conduction from the bottom in which energy transfer is limited through the bottom surface. Including heat conduction from the side walls would reduce the primary drying time, but only by a relatively small amount since the heat transfer area would still be limited. The temperature difference between the vial and its surroundings cannot be increased to counteract the limited heat transfer area because the high temperatures would damage the biotherapeutic material in the vial. By directly transmitted energy into the bulk material, microwave irradiation can produce

greatly reduced primary drying times without requiring large temperature gradients in the vial.

## 5. Conclusion

This numerical study is the first to explore the combination of applying microwave irradiation and thermal heat conduction to the freeze-drying for biopharmaceuticals. Compared to CFD, which is a time-consuming process taking many hours, MFD and HFD reduced the primary drying time by 78% and 83%, respectively, which are substantial time savings. This study establishes an MFD model that captures the main elements observed in the published experimental data, and proposes an HFD model suitable for the early-stage design of freeze-drying equipment that uses both conventional and microwave heating to accelerate the primary drying time by a factor of five over CFD. While both energy transfer methods contribute to the reduced primary drying time for HFD, parametric sensitivity analysis confirmed that the primary drying time is mainly dominated by microwave power rather than parameters associated with the heat transfer from the bottom of the vial. The mechanistic model assists in the fundamental understanding of MFD while having a low enough computational cost to be amenable to real-time nonlinear model predictive control implementation.

## Author contribution statement

**Jinwoo Park:** Conceptualization, Methodology, Software, Writing – Original Draft, Writing – Review & Editing, Visualization

**Jae Hyun Cho:** Writing – Review & Editing, Project administration, Funding acquisition

**Richard D. Braatz:** Conceptualization, Methodology, Writing – Original Draft, Writing – Review & Editing, Supervision, Project administration

## Declaration of Competing Interest

The authors declare that they have no known competing financial interests or personal relationships that could have appeared to influence the work reported in this paper.

## Acknowledgments

This work was supported by the “Program of Fostering Innovative Global Leaders” of the Korea Institute for Advancement of Technology (KIAT) with financial support by the Ministry of Trade, Industry & Energy (MOTIE), Republic of Korea (P0008747).

## Appendix

Assume that the temperature of the frozen region satisfies

$$T_2 = ax^2 + bx + c(t) \tag{A1}$$

where $a$ and $b$ denotes constant, and $c(t)$ denotes function of time.

Insertion of this expression into equation (22) gives

$$\rho_2 \hat{c}_{p_2} \frac{\partial\left(ax^2 + bx + c(t)\right)}{\partial t} = k_2 \frac{\partial^2\left(ax^2 + bx + c(t)\right)}{\partial x^2} + H_w p_{bw}^0 \tag{A2}$$

$$\rho_2 \hat{c}_{p_2} c\prime(t) = 2ak_2 + H_w p_{bw}^0 \tag{A3}$$

The insertion of the expression (A1) into the boundary condition (23) and equation (19),

$$-k_2 \frac{\partial T_2}{\partial x} = H_b \text{ at } t > 0, \ x = L \tag{23}$$

$$H_b = h\left(T_{shelf} - T_{bottom}\right) \tag{19}$$

results in

$$-k_2(2aL + b) = h\left[T_{shelf}(t) - \left(aL^2 + bL + c(t)\right)\right] \tag{A4}$$

$$c\prime(t) = -T\prime_{\text{shelf}}(t) \tag{A5}$$

Then combining equations (A3) and (A5) gives

$$-\rho_2 \hat{c}_{p_2} T\prime_{shelf}(t) = 2ak_2 + H_w p_{bw}^0 \tag{A6}$$

The shelf temperature was taken to linearly rise according to the time from equation (26),

$$T_{shelf}(t) = rt + T_{shelf}^0 \tag{26}$$

This equation can be inserted into (A6) to give the value of $a$ of

$$a = -\frac{r\rho_2 \hat{c}_{p_2} + H_w p_{bw}^0}{2k_2} \tag{A7}$$

Insertion of (A1) into the boundary condition (24),

$$-k_2 \frac{\partial T_2}{\partial x} = 0 \text{ at } t > 0, \ x = 0 \tag{24}$$

results in

$$b = 0 \tag{A8}$$

Inserting equations (26), (A7), and (A8) into equation (A4) gives

$$-2aLk_2 = h\left[rt + T_{shelf}^0 + \frac{r\rho_2 \hat{c}_{p_2} + H_w p_{bw}^0}{2k_2} L^2 - c(t)\right] \tag{A9}$$

where

$$c(t) = \frac{2aLk_2}{h} + rt + T_{shelf}^0 + \frac{r\rho_2 \hat{c}_{p_2} + H_w p_{bw}^0}{2k_2} L^2 \tag{A10}$$

Finally, inserting the expressions for $a$, $b$, and $c(t)$ into (A1) gives an analytical expression for the temperature of frozen region that solves all of the equations described the simplified model in this appendix:

$$T_2 = -\frac{r\rho_2 \hat{c}_{p_2} + H_w p_{bw}^0}{2k_2}(x^2 - L^2) + \frac{2aLk_2}{h} + rt + T_{shelf}^0 \tag{A11}$$

## References

Ambros, S., Bauer, S.A.W., Shylkina, L., Foerst, P., Kulozik, U., 2016. Microwave-Vacuum Drying of Lactic Acid Bacteria: Influence of Process Parameters on Survival and Acidification Activity. Food Bioprocess Technol 9, 1901–1911. doi:10.1007/s11947-016-1768-0.

Badr, S., Sugiyama, H., 2020. A PSE perspective for the efficient production of monoclonal antibodies: integration of process, cell, and product design aspects. Curr. Opin. Chem. Eng. 27, 121–128. doi:10.1016/j.coche.2020.01.003.

Capozzi, L.C., Trout, B.L., Pisano, R., 2019. From Batch to Continuous: Freeze-Drying of Suspended Vials for Pharmaceuticals in Unit-Doses. Ind. Eng. Chem. Res. 58, 1635–1649. doi:10.1021/acs.iecr.8b02886.

Casola, G., Siegmund, C., Mattern, M., Sugiyama, H., 2019. Data mining algorithm for pre-processing biopharmaceutical drug product manufacturing records. Comput. Chem. Eng. 124, 253–269. doi:10.1016/j.compchemeng.2018.12.001.

Colucci, D., Fissore, D., Barresi, A.A., Braatz, R.D., 2020. A new mathematical model for monitoring the temporal evolution of the ice crystal size distribution during freezing in pharmaceutical solutions. Eur. J. Pharm. Biopharm. 148, 148–159. doi:10.1016/j.ejpb.2020.01.004.

de Jesus, S.S., Filho, R.M., 2011. Optimizing drying conditions for the microwave vacuum drying of enzymes. Dry. Technol. 29, 1828–1835. doi:10.1080/07373937.2011.605977.

Eberle, L., Capón-García, E., Sugiyama, H., Graser, A., Schmidt, R., Hungerbühler, K., 2016. Rigorous approach to scheduling of sterile drug product manufacturing. Comput. Chem. Eng. 94, 221–234. doi:10.1016/j.compchemeng.2016.07.028.

Fan, K., Zhang, M., Mujumdar, A.S., 2019. Recent developments in high efficient freeze-drying of fruits and vegetables assisted by microwave: A review. Crit. Rev. Food Sci. Nutr. 59, 1357–1366. doi:10.1080/10408398.2017.1420624.

Farrel, G., McMinn, W.A.M., Magee, T.R.A., 2005. Microwave-vacuum drying kinetics of pharmaceutical powders. Dry. Technol. 23, 2131–2146. doi:10.1080/07373930500212354.

Fissore, D., Pisano, R., Barresi, A., 2019. Freeze Drying of Pharmaceutical Products. CRC Press doi:10.1201/9780429022074.

Giordano, A., Barresi, A.A., Fissore, D., 2011. On the use of mathematical models to build the design space for the primary drying phase of a pharmaceutical lyophilization process. J. Pharm. Sci. 100, 311–324. doi:10.1002/jps.22264.
Gitter, J.H., Geidobler, R., Presser, I., Winter, G., 2019. Microwave-assisted freeze-drying of monoclonal antibodies: Product quality aspects and storage stability. Pharmaceutics 11, 9–12. doi:10.3390/pharmaceutics11120674.
Gitter, J.H., Geidobler, R., Presser, I., Winter, G., 2018. Significant Drying Time Reduction Using Microwave-Assisted Freeze-Drying for a Monoclonal Antibody. J. Pharm. Sci. 107, 2538–2543. doi:10.1016/j.xphs.2018.05.023.
Hong, M.S., Severson, K.A., Jiang, M., Lu, A.E., Love, J.C., Braatz, R.D., 2018. Challenges and opportunities in biopharmaceutical manufacturing control. Comput. Chem. Eng. 110, 106–114. doi:10.1016/j.compchemeng.2017.12.007.
Hottot, A., Peczalski, R., Vessot, S., Andrieu, J., 2006. Freeze-drying of pharmaceutical proteins in vials: Modeling of freezing and sublimation steps. Dry. Technol. 24, 561–570. doi:10.1080/07373930600626388.
Kappatou, C.D., Ehsani, A., Niedenführ, S., Mhamdi, A., Schuppert, A., Mitsos, A., 2020. Quality-targeting dynamic optimization of monoclonal antibody production. Comput. Chem. Eng. 142, 107004. doi:10.1016/j.compchemeng.2020.107004.
Kawasaki, H., Shimanouchi, T., Kimura, Y., 2019. Recent Development of Optimization of Lyophilization Process. J. Chem. 2019, 9502856. doi:10.1155/2019/9502856.
Kumar, A., Singh, A., Singh, R., Misra, A., 2020. Remdesivir in COVID-19: A critical review of pharmacology, pre-clinical and clinical studies. Diabetes Metab. Syndr. Clin. Res. Rev. 14, 641–648. doi:10.1016/j.dsx.2020.05.018, https://doi.org/https://doi.org/.
Langford, A., Bhatnagar, B., Walters, R., Tchessalov, S., Ohtake, S., 2018. Drying technologies for biopharmaceutical applications: Recent developments and future direction. Dry. Technol. 36, 677–684. doi:10.1080/07373937.2017.1355318.
Liapis, A.I., Bruttini, R., 1995. Freeze-Drying of pharmaceutical crystalline and amorphous solutes in vials: Dynamic multi-dimensional models of the primary and secondary drying stages and qualitative features of the moving interface. Dry. Technol. 13, 43–72. doi:10.1080/07373939508916942.
Litchfield, R.J., Liapis, A.I., 1979. An adsorption-sublimation model for a freeze dryer. Chem. Eng. Sci. 34, 1085–1090. doi:10.1016/0009-2509(79)85013-7.
Liu, S., Papageorgiou, L.G., 2018. Multi-objective optimisation for biopharmaceutical manufacturing under uncertainty. Comput. Chem. Eng. 119, 383–393. doi:10.1016/j.compchemeng.2018.09.015.
Mascarenhas, W.J., Akay, H.U., Pikal, M.J., 1997. A computational model for finite element analysis of the freeze-drying process. Comput. Methods Appl. Mech. Eng. 148, 105–124. doi:10.1016/S0045-7825(96)00078-3.
Matsunami, K., Miyano, T., Arai, H., Nakagawa, H., Hirao, M., Sugiyama, H., 2018. Decision Support Method for the Choice between Batch and Continuous Technologies in Solid Drug Product Manufacturing. Ind. Eng. Chem. Res. 57, 9798–9809. doi:10.1021/acs.iecr.7b05230.
Matzler, C., 1987. Dielectric Properties of Fresh-Water Ice at Microwave Frequencies. J. Phys. D Appl. Phys. 20, 1623. doi:10.1088/0022-3727/20/12/013.
McMinn, W.A.M., Farrell, G., Magee, T.R.A., 2007. Prediction of microwave drying behavior of pharmaceutical powders using thin-layer models. Dry. Technol. 25, 1551–1569. doi:10.1080/07373930701539761.
Millman, M.J., Liapis, A.I., Marchello, J.M., 1985. An analysis of the lyophilization process using a sorption-sublimation model and various operational policies. AIChE J 31, 1594–1604. doi:10.1002/aic.690311003.
Muzzio, C.R., Dini, N.G., 2011. Simulation of freezing step in vial lyophilization using finite element method. Comput. Chem. Eng. 35, 2274–2283. doi:10.1016/j.compchemeng.2010.10.009.
Nagy, Z.K., Braatz, R.D., 2011. Nonlinear model predictive control for batch processes. The Control Handbook, 2nd edition CRC Press Control System Applications, Chapter 15.
Papathanasiou, M.M., Burnak, B., Katz, J., Shah, N., Pistikopoulos, E.N., 2019. Assisting continuous biomanufacturing through advanced control in downstream purification. Comput. Chem. Eng. 125, 232–248. doi:10.1016/j.compchemeng.2019.03.013.
Park, K.S., Sun, X., Aikins, M.E., Moon, J.J., 2021. Non-viral COVID-19 vaccine delivery systems. Adv. Drug Deliv. Rev. 169, 137–151. doi:10.1016/j.addr.2020.12.008.
Pikal, M.J., Cardon, S., Bhugra, C., Jameel, F., Rambhatla, S., Mascarenhas, W.J., Akay, H.U., 2005. The nonsteady state modeling of freeze drying: In-process product temperature and moisture content mapping and pharmaceutical product quality applications. Pharm. Dev. Technol. 10, 17–32. doi:10.1081/PDT-200035869.
Pisano, R., Arsiccio, A., Capozzi, L.C., Trout, B.L., 2019. Achieving continuous manufacturing in lyophilization: Technologies and approaches. Eur. J. Pharm. Biopharm. 142, 265–279. doi:10.1016/j.ejpb.2019.06.027.
Sadikoglu, H., Liapis, A.I., 1997. Mathematical modelling of the primary and secondary drying stages of bulk solution freeze-drying in trays: Parameter estimation and model discrimination by comparison of theoretical results with experimental data. Dry. Technol. 15, 791–810. doi:10.1080/07373939708917262.
Severson, K., VanAntwerp, J.G., Natarajan, V., Antoniou, C., Thömmes, J., Braatz, R.D., 2015. Elastic net with Monte Carlo sampling for data-based modeling in biopharmaceutical manufacturing facilities. Comput. Chem. Eng. 80, 30–36. doi:10.1016/j.compchemeng.2015.05.006.
Sheehan, P., Liapis, A.I., 1998. Modeling of the primary and secondary drying stages of the freeze drying of pharmaceutical products in vials: Numerical results obtained from the solution of a dynamic and spatially multi-dimensional lyophilization model for different operational policies. Biotechnol. Bioeng. 60, 712–728. doi:10.1002/(SICI)1097-0290(19981220)60:6⟨712::AID-BIT8⟩3.0.CO;2-4.
Velardi, S.A., Barresi, A.A., 2008. Development of simplified models for the freeze-drying process and investigation of the optimal operating conditions. Chem. Eng. Res. Des. 86, 9–22. doi:10.1016/j.cherd.2007.10.007.
Walters, R.H., Bhatnagar, B., Tchessalov, S., Izutsu, K.I., Tsumoto, K., Ohtake, S., 2014. Next generation drying technologies for pharmaceutical applications. J. Pharm. Sci. 103, 2673–2695. doi:10.1002/jps.23998.
Witkiewicz, K., Nastaj, J.F., 2010. Simulation strategies in mathematical modeling of microwave heating in freeze-drying process. Dry. Technol. 28, 1001–1012. doi:10.1080/07373937.2010.497090.